ELSEVIER

Chemical Geology 186 (2002) 57–73

CHEMICAL GEOLOGY
INCLUDING
ISOTOPE GEOSCIENCE

www.elsevier.com/locate/chemgeo

Solving the production–diffusion equation for finite diffusion domains of various shapes
Part II. Application to cases with α-ejection and nonhomogeneous distribution of the source

A.G.C.A. Meesters, T.J. Dunai*

Faculty of Earth Sciences, Vrije Universiteit, De Boelelaan 1085, 1081 HV Amsterdam, The Netherlands

Received 30 May 2001; accepted 6 December 2001

Abstract

In this paper, numerical methods derived in Part I (Chem. Geol. (2002)) are expanded to accommodate the effects of α-emission and zonation of U and Th as relevant for (U–Th)/He thermochronology. Expressions for the required coefficients are derived for spheres, finite and infinite cylinders and rectangular blocks, for parent nuclide distributions, which are either uniform or have stepwise zoning. We show that the effects of α-emission and zonation on the He retention in a nonspherical crystal of modest aspect ratio can be approximated by a sphere of identical surface-to-volume ratio (S/V) if the zonation is transposed on to the sphere. The currently usual correction method is to perform first a diffusive calculation without considering α-emission and zonation and to multiply afterward with a correction factor that has been derived originally for nondiffusive calculations. Our results demonstrate that more accurate calculations yield different results and that the differences are often too large to be ignored in practice. Especially for thermal histories that include a protracted residence in the partial retention zone, the difference between the usual correction and our correction can be as high as ~ 20% for homogeneous sources. For zoned crystals, the difference can be even larger.

Keywords: Low-temperature thermochronology; Diffusion; Forward modelling; Zonation; Alpha emission; (U–Th)/He dating

1. Introduction

In Part I (Meesters and Dunai, in press), an efficient algorithm has been presented for calculating the ^{4}He accumulation from the decay of U and Th in crystals of various shapes for a given thermal history. The algorithm is based on decomposition of the He content into eigenmodes of the Laplace operator. However, the method of Part I was incomplete in two respects. First, a homogeneous distribution of the parent nuclides over the crystal was assumed, whereas heterogeneous (especially zonal) distributions are often encountered in practice. Second, the algorithm did not account for the long stopping distances of the emitted α-particles. This distance, σ, is, for instance, about 20 μm in apatite (Farley et al., 1996; Ziegler, 1977), which is too long to be neglected in practice. It is clear that the He content is depleted by this effect

* Corresponding author. Fax: +31-6462457.
E-mail address: dunt@geo.vu.nl (T.J. Dunai).

0009-2541/02/$ - see front matter
PII: S0009-2541(01)00423-5

close to the margin since part of the α-particles leave the crystal. Farley et al. (1996) have discussed how to correct for this effect in the absence of diffusion. In the presence of diffusion, it is currently customary to first perform calculations with a diffusion model for a (spherical) crystal with a simple homogenous source and, subsequently, multiply the result with a correction factor for α-ejection (e.g. House et al., 1999; Stockli et al., 2000; Warnock et al., 1997). However, it is evident that this is a simplification, as the outcome of a correct production–diffusion calculation does not only depend on the amount of He produced, but also on the spatial distribution of the He (Farley, 2000). For instance, in the simplest case (no zonation), the He is relatively strongly depleted in the outer parts due to α-ejection and this, in turn, will decrease the relative degree of diffusive loss of He as compared to a rectangular concentration profile that would be valid in the absence of α-ejection. As a result, the conventionally corrected ages are generally overcorrected if diffusion is important. The two processes, α-ejection and diffusion, are interwoven and a new algorithm is required that incorporates both processes simultaneously.

This more involved exercise is more than of academic interest as apatites with strongly zoned U distribution (and by inference also Th) are frequently encountered in fission track analysis and do occur in apatites of plutonic, volcanic and metamorphic provenance (members of the fission track group at the Vrije Universiteit Amsterdam, personal communication, e.g. see Fig. 1). The occurrence of zonation cannot be predicted (some populations are not zoned), but must be established for each apatite sample. Concentration contrasts between inner and outer regions in a crystal may range 1–2 orders of magnitude such that the U (Th)-rich portion inevitably will dominate the He accumulation history as we try to reconstruct in our analytical work. It is beyond the scope of this paper to discuss analytical techniques that allow to identify and to characterise U–Th zonations in the apatite grains used for analysis in (U–Th)/He thermochronology. Suitable analytical techniques are currently developed at the Vrije Universiteit Amsterdam.

In the present paper, an algorithm is presented for predicting He contents from thermal histories, taking into account the combined effects of long stopping distances of α-particles, heterogeneous distribution of the parent nuclides and diffusion. It is understood that the reader is acquainted with the methods of Part I. The algorithm is actually identical to the one of Part I, except for the fact that the coefficients that we called γ-coefficients have to be adapted. The methods in Section 2 is, apart from an introductory subsection (Section 2.1) and a subsection with general directions (Section 2.2), entirely devoted to the problem of calculating these γ-coefficients.

The methods to calculate γ-coefficients depend strongly on the geometry. For spherical crystals, it is fortunately possible to find analytical expressions (Sections 2.5 and 2.6). Moreover, for spherical crystals, only few eigenmodes have to be incorporated in the calculations to obtain accurate results, making the algorithm much faster than for other shapes. Real crystals are not spherical, but it was our hope that "arbitrary" crystals could be "translated" to equivalent spherical crystals. It is shown in Section 3 that this can indeed be done by taking spheres with the same surface-to-volume ratio (S/V) and similar zoning, provided the crystals are not too elongated and provided the U–Th zonations have shapes in accordance with the crystal shape. The best agreements are found between spheres and finite cylinders, which is particulary useful for apatite. With this background, the methods for spheres that are given here are probably much more useful than the methods for other shapes. These latter methods had, of course, also to be described since they are used here for comparison.

In Section 3, we also give attention to the question whether work can be saved by using "shortcuts", such as replacing an inhomogeneous distribution by a homogeneous one, or applying correction coefficients for α-ejection, as found by calculations for nondiffusive cases, to diffusive cases. It will be shown that

Fig. 1. Photomicrographs of apatite grains and the corresponding mica external detectors as used in fission track analysis. Visible are the etched tracks created by spontaneous and induced fission of ^{238}U and ^{235}U, respectively. The track density within the zones of a grain/external monitor image is proportional to the U–concentration. (a) Vassijaur granite, Sweden; 68°25′ 16″N 18°07′ 42″E; (b) Skröven granites, Sweden, 66°18′ 43″N 22°48′ 55″E; (c) gneis, Baisvarri complex, Sweden 70°03′ 57″N 27°44′ 18″E. Photos courtesy of Bart Hendriks.

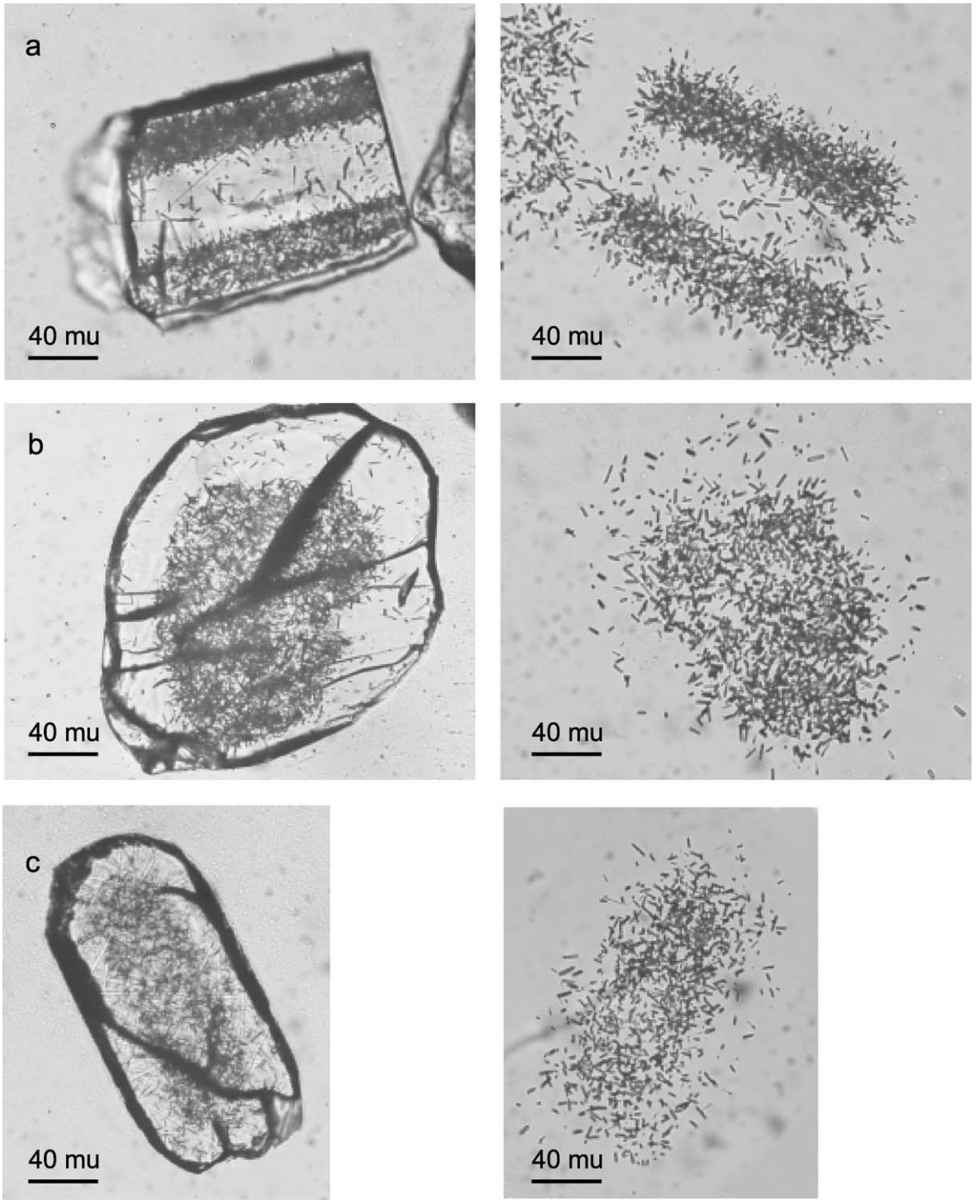
a
40 mu
40 mu
b
40 mu
40 mu
c
40 mu
40 mu

either of these simplifications leads, in general, to large systematic errors.

2. Methods

2.1. Model description

For the generation of helium in a crystal, the following model is assumed (Farley et al., 1996). The parent nuclides are distributed (not necessarily homogeneously) over the crystal and we write the corresponding density of α-emission as $U_{\mathrm{place}}(x,y,z)U_{\mathrm{R}}(t)$, in which $U_{\mathrm{R}}(t)$ is the total α-production divided by the total crystal volume, and $U_{\mathrm{place}}(x,y,z)$ is a dimensionless distribution with a volume average of one. In the following, other quantities will also be chosen dimensionless if possible. If an α-particle is produced at a point, it is emitted in entirely arbitrary direction and comes to rest at a distance, σ, at a point that may be within or outside the crystal.

Farley et al. (1996) employ a function $F(x,y,z)$, which is the chance that an α-particle emitted at (x,y,z) remains within the crystal. F does not indicate how the new He is distributed spatially. We use the dimensionless function $S_{\mathrm{place}}(x,y,z)$ to denote the chance, per volume unit and multiplied with the total crystal volume, that an emitted α-particle stops at (x,y,z). Consequently, the source term in the production–diffusion equation is $S_{\mathrm{place}}(x,y,z)U_{\mathrm{R}}(t)$. S_{place} depends on the crystal geometry, on the parent distribution, U_{place}, and on the stopping distance, σ.

Mathematically, $S_{\mathrm{place}}(x,y,z)$ is calculated by taking the average of U_{place} over an infinitely thin spherical shell with center (x,y,z) and radius σ, assuming $U_{\mathrm{place}}=0$ outside the crystal. $F(x,y,z)$ is calculated by taking the average over the same shell of a function, which is one inside and zero outside the crystal. In the special case that $U_{\mathrm{place}}=1$ (homogeneous distribution of the parent nuclide), $F=S_{\mathrm{place}}$.

The retentivity, F_{T}, which is the probability that an emitted α-particle stops within the crystal, can be expressed in two ways:

$$F_{\mathrm{T}} = \frac{1}{V}\int \mathrm{d}V\, S_{\mathrm{place}}(x,y,z) = \frac{1}{V}\int \mathrm{d}V\, U_{\mathrm{place}}(x,y,z)F(x,y,z). \quad (1)$$

The second form was used by Farley et al. (1996), the first yields the same result though, locally, $S_{\mathrm{place}} \neq U_{\mathrm{place}}F$.

The fundamental quantities have now been given; it remains to be considered how the evolution of the He content, $C_{\mathrm{av}}(t)$, in the presence of diffusion can be calculated from them.

2.2. How the evolution of the Helium content is calculated

It has been derived in Appendix A of Part I that for any He source, $S_{\mathrm{place}}(x,y,z)U_{\mathrm{R}}(t)$, the spatial average $C_{\mathrm{av}}(t)$ of the He concentration evolves as:

$$C_{\mathrm{av}}(t) = \sum_{n=1}^{\infty} c_n(t), \quad (2)$$

with $c_n(t)$ governed by:

$$\frac{\mathrm{d}c_n}{\mathrm{d}t} = -\mu_n D(t) c_n(t) + \gamma_n U_{\mathrm{R}}(t), \quad (3)$$

where D is the diffusion coefficient. Herein, μ_n depends only on the geometry and has been treated in Part I. However, γ_n has to be adapted to S_{place}. Once γ_n is known (for an array of low n values), the numerical solution of the differential equations for each $c_n(t)$ and the summing of the $c_n(t)$ can be performed as described in Part I. Thus, the whole specific problem caused by α-emission and heterogeneity of the source is the determination of γ_n. This will occupy us in Sections 2.3–2.7.

An important result (dealt with in Sections 2.5 and 2.6) is that analytical expressions for γ_n can be found for the sphere, if the distribution of parent nuclides is homogeneous, or if it is a simple step function of the distance to the center. This special result has a wider scope of application than might be apparent at first, for the following reasons. First, the γ_n obey (just like S_{place} and C) the *superposition principle*: If arbitrary parent nuclides distributions $U^{(1)}(r)$ and $U^{(2)}(r)$ yield γ-values $\gamma_n{}^{(1)}$ and $\gamma_n{}^{(2)}$, respectively, for the nth eigenmode, then any arbitrary combination, say for instance, $U(r)=4U^{(1)}+7U^{(2)}$, yields the corresponding combination of γ-values: $\gamma_n=4\gamma_n{}^{(1)}+7\gamma_n{}^{(2)}$ (proof: that such a rule holds for S_{place} follows from its mathematical definition in Section 2.1; from Eq. (10) in Section 2.3, it follows subsequently for γ_n).

Since any $U(r)$ can be approximated by combining several step functions, its γ_n can be approximated by combining the corresponding analytical results. Second, as will be shown in Sections 3.1 and 3.2, the evolution of $C_{av}(t)$ for crystals with either homogeneous or zonal distribution of parent nuclides does not strongly depend on size and shape, but tends to be universal for a given zoning and surface-to-volume ratio. This implies that for a variety of crystal shapes, the evolution problem can be translated to an evolution problem on the sphere, for which the γ_n can be relatively easily obtained. Moreover, the γ_n for the sphere have only one index so that faster calculation is possible with them than with the γ_n for other finite shapes.

It must now be considered what is the use of F_T for diffusion calculations. We first note that:

$$\frac{dC_{av}}{dt} \leq F_T U_R, \tag{4}$$

with "=" in absence and "<" in presence of diffusion. Since the "measured age", t_c is C_{av}/U_R according to the customary definition, it follows (neglecting the time dependence of U_R) that:

$$\frac{dt_c}{dt} \leq F_T, \tag{5}$$

again with the same remark about = and <.

Clearly, for cases where diffusion is important, t_c has no simple relation to F_T. Further, as will be shown in Section 3, the often used method to apply F_T as correction factor in conjunction with diffusion calculations yields, in general, erroneous results. Still, determining F_T remains useful because of the following interesting identity:

$$F_T = \sum_n \gamma_n, \tag{6}$$

(summation over all eigenmodes). This identity is very useful for checking the validity and accuracy of results (and has been used time and again in checking the results in this paper).

The most fundamental way to prove this relation is the following. For the nondiffusive case, we have Eq. (4) with "=" sign; however, on the other hand, dC_{av}/dt can be determined from Eqs. (2) and (3) with $D(t)=0$ substituted. Combining both outcomes yields Eq. (6). This relation connects crystal characteristics and holds independent of the nature of thermal evolution.

2.3. Calculation of γ_n: general remarks

This subsection can be skipped by readers who are not interested in derivations. We now consider how the calculation of the γ-coefficients has to be adjusted if α-emission and eventually inhomogeneous U_{place} are to be taken into account. As was discussed already in Appendix A of Part I, the γ_n are derived from the eigenfunctions μ_n of the Laplace operator which are zero at the crystal boundary, as follows:

$$\gamma_n = s_n \mu_{n,av}, \tag{7}$$

in which $\mu_{n,av}$ is the volume average of μ_n, and the s_n are the expansion coefficients of S_{place}:

$$S_{place}(x,y,z) = \sum_n s_n \mu_n(x,y,z). \tag{8}$$

It follows from the general principles of eigenfunction theory (see, e.g. Collins, 1968, Chapter 5) that:

$$s_n = \int dV\, S_{place}\mu_n \Big/ \int dV(\mu_n)^2 \tag{9}$$

Hence:

$$\gamma_n = \frac{1}{V}\frac{\int dV \mu_n}{\int dV(\mu_n)^2} \int dV\, S_{place}\mu_n. \tag{10}$$

The integrals that do not involve S_{place} can be looked up in Carslaw and Jaeger (1959). The integral containing S_{place} is a different story. Though analytical results can be obtained for the sphere (see Sections 2.5 and 2.6), usually numerical integration has to be performed.

2.4. Calculation of γ_n: special cases

As this subsection is again only about derivations, it may also be skipped. The sphere with radius, a, appears to be in every respect the easiest shape to work with. It is assumed that the parent nuclide distribution (and, hence, S_{place}) depends on the dis-

tance, r, to the center alone. In the expansion of S_{place} in eigenfunctions, only eigenfunctions with the same symmetry will occur; these are:

$$\mu_n(r) = \frac{1}{r}\sin\left(n\pi\frac{r}{a}\right) \tag{11}$$

with $n = 1, 2, 3, \ldots$ (note that μ_n is regular in $r = 0$). The expressions for γ_n and F_{T}, obtained with Eqs. (1) and (10), are:

$$\gamma_n = (-1)^{n+1}\frac{6}{n\pi}\frac{1}{a^2}\int_0^a \mathrm{d}r\ r^2 S_{\text{place}}(r)\mu_n(r), \tag{12}$$

$$F_{\text{T}} = \frac{3}{a^3}\int_0^a \mathrm{d}r\ r^2 S_{\text{place}}(r). \tag{13}$$

Analytical solution is, in general, possible for the sphere; this will be discussed in Sections 2.5 and 2.6 and readers may proceed by reading there.

For crystals of other shapes, analytical solutions are, in general, out of scope. It will even be hard to find S_{place} analytically. However, it is always possible to estimate S_{place} by a Monte Carlo method. This amounts to the following: to determine S_{place} at a given point (x,y,z), one emits for a number of times an α-particle from there "back" to a point (x',y',z') at a distance, σ, and in a fully random direction. For each experiment, one determines the value of $U_{\text{place}}(x',y',z')$; if the point is outside the crystal, the value zero is assigned. Then the average outcome of all experiments is determined; this is the estimate for $S_{\text{place}}(x,y,z)$.

For completeness, we give a prescript to achieve this numerically. With a random number generator, one can produce numbers u and v that have a uniform distribution between 0 and 1. From them, one calculates polar angles, θ and φ:

$$\theta = \arccos(1-2u); \quad \varphi = 2\pi v. \tag{14}$$

These are just distributed such that the corresponding direction is random. For the stopping point (x,y,z), the potential point of emission (x',y',z') is:

$$\begin{aligned} x' &= x + \sigma\sin\theta\cos\varphi; \quad y' \\ &= y + \sigma\sin\theta\sin\varphi; \quad z' = z + \sigma\cos\theta. \end{aligned} \tag{15}$$

For the block with x from 0 to a, y from 0 to b, and z from 0 to c, the concerned eigenfunctions are (eigenfunctions with odd symmetry do not contribute):

$$\begin{aligned} \mu_{lmn}(x,y,z) = \sin\left((2l-1)\pi\frac{x}{a}\right)\sin\left((2m-1)\pi\frac{y}{b}\right) \\ \times \sin\left((2n-1)\pi\frac{z}{c}\right). \end{aligned} \tag{16}$$

It is straight forward to write a program for obtaining F_{T} and γ_{lmn} (with the required S_{place} determined by the Monte Carlo method); however, computations are relatively time-consuming since three-dimensional integrals are involved (though one can somewhat reduce the required computational effort by using tricks based on the symmetry of the problem). Worse is that the number of γ-coefficients becomes so large, a problem already discussed in Part I.

The cylinder with radius, a, and height, h, has eigenfunctions that contain the Bessel function, J_0. Hence, some extra effort is required to write down algorithms for the computation of F_{T} and γ_{mn}. On the other hand, once the programs can be run, they are relatively attractive since there are only two indices instead of three.

For the cylinder, the eigenfunctions are (assuming a cylindrical symmetry for the distribution of parent nuclides):

$$\mu_{mn}(r,z) = J_0\left(j_m\frac{r}{a}\right)\sin\left((2n-1)\pi\frac{z}{h}\right). \tag{17}$$

Herein, m and n run from 1 to ∞, J_0 is a Bessel function and j_m is its mth zero point. The expressions for γ_{mn} and F_{T} are:

$$\begin{aligned} \gamma_{m,n} = -\frac{16}{\pi a^2 h n j_m J_0'(j_m)}\int_0^h \mathrm{d}z\int_0^a \mathrm{d}r\ rS_{\text{place}}(r,z) \\ \times J_0(j_m r/a)\sin((2n-1)\pi z/h), \end{aligned} \tag{18}$$

$$F_{\text{T}} = \frac{2}{a^2 h}\int_0^h \mathrm{d}z\int_0^a \mathrm{d}r\ rS_{\text{place}}(r,z). \tag{19}$$

To determine S_{place}, the Monte Carlo method can again be used. If values of j_m , $J_0'(j_m)$ and $J_0(\ldots)$ cannot be determined using numerical software already available, the necessary information can be found in Abramowitz and Stegun (1965): values of j_m and $J_0'(j_m)$ are found in Table 9.5 of that book (trans-

late $j_m = j_{m,0}$) and an accurate approximation to evaluate J_0 is given in Section 9.4 of the same book.

For the cylinder of infinite length, only one index remains:

$$\gamma_m = -\frac{4}{a^2 j_m J_0'(j_m)} \int_0^a \mathrm{d}r\ r S_{\mathrm{place}}(r) J_0(j_m r/a), \tag{20}$$

$$F_{\mathrm{T}} = \frac{2}{a^2} \int_0^a \mathrm{d}r\ r S_{\mathrm{place}}(r). \tag{21}$$

2.5. Calculation of γ_n: sphere with homogeneous distribution of parent nuclides

We first continue with the derivation for the sphere, and then give the results for F_{T} and γ. In Appendix A, the following expression for S_{place} is derived for the sphere (Eq. (34)):

$$S_{\mathrm{place}}(r) = \frac{1}{2\sigma r} \int_{|r-\sigma|}^{r+\sigma} \mathrm{d}s\ s U_{\mathrm{place}}(s). \tag{22}$$

For homogeneous distribution of the parent nuclides, $U_{\mathrm{place}}(s) = 1$ for $s < a$, and as always $U_{\mathrm{place}}(s) = 0$ for $s > a$. We note that a point P in a crystal can be of three types: Of the points P' at a distance, σ, away from P, (1) all or (2) some or (3) none may be situated within the crystal. The third option can only occur for small crystals ($a < \sigma$). In accordance with this, the result of the integral for $S_{\mathrm{place}}(r)$ can have three forms, depending on whether a is situated above, or within, or below the interval from $|r-\sigma|$ to $r+\sigma$:

$$S_{\mathrm{place}}(r) = 1 \qquad (a \geq r + \sigma),$$

$$S_{\mathrm{place}}(r) = (a^2 - |r-\sigma|^2)/(4\sigma r) \times (|r-\sigma| < a < r+\sigma), \tag{23}$$

$$S_{\mathrm{place}}(r) = 0 \qquad (a \leq |r+\sigma|).$$

This result is also found in Farley et al. (1996).

From this, expressions for γ_n and F_{T} can be obtained with Eqs. (11–13. Provided $a > \sigma/2$ (otherwise $\gamma_n = 0$):

$$n = \frac{3}{(n\pi)^2} \times \left(1 - \frac{\sigma}{2a} + \frac{1}{n\pi}\frac{1}{k\sigma}(1 - \cos(k\sigma)) + \frac{1}{k\sigma}\sin(k\sigma)\right), \tag{24}$$

in which k depends on n according to:

$$k = n\pi/a. \tag{25}$$

This is a very manageable result. Further, as mentioned earlier by Farley et al. (1996):

$$F_{\mathrm{T}} = 1 - \frac{3}{4}\frac{\sigma}{a} + \frac{1}{16}\frac{\sigma^3}{a^3} \tag{26}$$

again provided $a > \sigma/2$ (otherwise $F_{\mathrm{T}} = 0$). We have performed an independent check on Eq. (24) by verifying that $\sum \gamma_n = F_{\mathrm{T}}$, using analytical expressions for the concerned sums (Abramowitz and Stegun, 1965, numbers 23.1.17–18 and 23.2.24–25).

2.6. Calculation of γ_n: sphere with zoned distribution of parent nuclides

For nonhomogeneous $U(r)$, the computations become more involved. It is discussed in Appendix A how the analysis can be facilitated. The analysis has to work with a double integral, with integration both over points of emission and over points where the α-particles come to rest. In the following, by the contribution of a region to γ_n and F_{T} , we mean the contribution of the α-particles emitted, not those that came to rest in that region.

We apply this analysis now to the special case that $U(r)$ is a step function and, hence, can be written as a combination of functions which are constant on a shell. A shell $p \leq r \leq q$ on which $U(r) = U_0$ (see Fig. 2) yields a contribution to γ_n and F_{T}, the expression of which will depend on the region in which the shell lies, and the definitions of the involved regions depend on their turn on the ratio of σ to a.

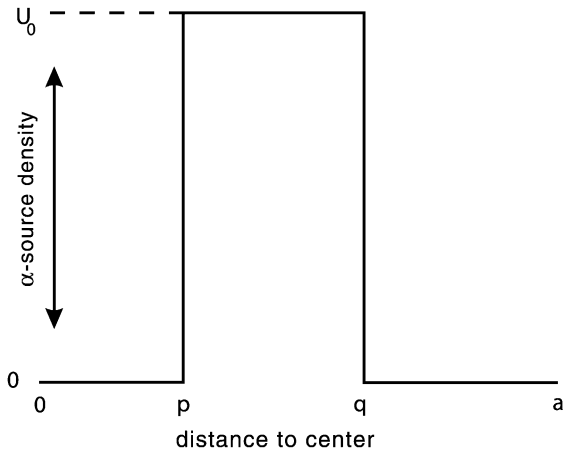

Fig. 2. Illustration of a step distribution of the α-source, explaining the symbols used in the text.

We first consider the most important (and most complicated) case, namely the case that $\sigma \le a$. One has then to discern between an outer region $a - \sigma \le r \le a$, and an inner region $r \le a - \sigma$. If the shell lies in the outer region, it yields the following contributions:

$$\gamma_{n,\text{outer}} = \frac{3}{(n\pi)^4}\frac{aU_0}{\sigma}\left[\frac{q^2-p^2}{2}k^2 + (-1)^{n+1} \times [kq\sin k(q-\sigma) - kp\sin k(p-\sigma) + \cos k(q-\sigma) - \cos k(p-\sigma)]\right], \quad (27)$$

in which

$$k = \frac{n\pi}{a}$$

again contains the dependence on n, and

$$F_{T,\text{outer}} = \frac{U_0}{a^3}\left[\frac{q^3-p^3}{2} + \frac{3}{8\sigma}\left(a^2 - \sigma^2 - \frac{p^2+q^2}{2}\right) \times (q^2-p^2)\right]. \quad (28)$$

If, on the other hand, the shell lies in the inner region, the contributions become

$$\gamma_{n,\text{inner}} = (-1)^{n+1}\frac{6}{(n\pi)^4}\frac{aU_0}{\sigma}\sin(k\sigma)[kp\cos(kp) - kq\cos(kq) + \sin(kq) - \sin(kp)], \quad (29)$$

$$F_{T,\text{inner}} = \frac{U_0}{a^3}(q^3 - p^3). \quad (30)$$

If $a < \sigma \le 2a$, there are again two regions, namely an outer region $\sigma - a \le r \le a$, and an inner region $r \le \sigma - a$. A shell in the outer region yields contributions of just the same form as for the case $\sigma < a$ considered above. A shell in the inner region yields no contribution now since all α-particles emitted there leave the crystal. If finally $\sigma > 2a$, all α-particles are ejected out of the crystal, and γ_n and F_T are zero.

2.7. A note on the calculation of γ_n without α-emission

We have not performed calculations for the case that α-emission is absent; however, zoning is present in the crystals (e.g. for Ar-geochronology) since our intentions are restricted to analysing measurements with α-emission. Actually, without α-emission the calculations are easier. A brief sketch is as follows. In Section 2.4, "S_{place}" should everywhere be replaced with "U_{place}". Thereby, integrals are obtained that are of a kind that is treated by Carslaw and Jaeger (1959). If U_{place} has the character of a step function, it is possible to obtain analytical expressions for γ for all the usual shapes. However, for cylindrical shapes, these expressions contain Bessel functions.

3. Results

3.1. Results for homogeneous distribution of parent nuclides

In Part I, we calculated the evolution of the He ages for five thermal histories (taken from Wolf et al., 1998) and five crystal shapes with $S/V = 0.05\ \mu\text{m}^{-1}$. The same exercise has been done now with α-emission

included, using the methods of Section 2.2, with γ-coefficients calculated according to Section 2.5 for the sphere, and to Section 2.4 for the other shapes (finite and infinite cylinder, rectangular block and cube).

The source distribution of the α-particles is kept homogeneous; nonhomogeneous distributions will be considered in Section 3.2. For the stopping length, a mean value of $\sigma = 20$ μm is assumed (Farley et al., 1996). A grid distance of 1 μm is used in performing the numerical calculation of γ_n and F_T. In applying the Monte Carlo method, each time 100 random emission directions are considered. The thermal histories (as in Part I) will be indicated in the figures. The dimensions are again chosen to yield identical S/V-ratio and are as follows: sphere: radius 60 μm; cube: edges 120 μm; block: edges 80, 160, 160 μm; finite cylinder: radius 50 μm, height 200 μm; infinite cylinder: radius 40 μm. The time step is again 5 Ma (but 1 Ma for the final stage of history 5). As in Part I, a slight adjustment is made to deal with a discontinuous temperature.

Fig. 3a shows the results for history 1, with a sudden shift from high to low temperature. For this

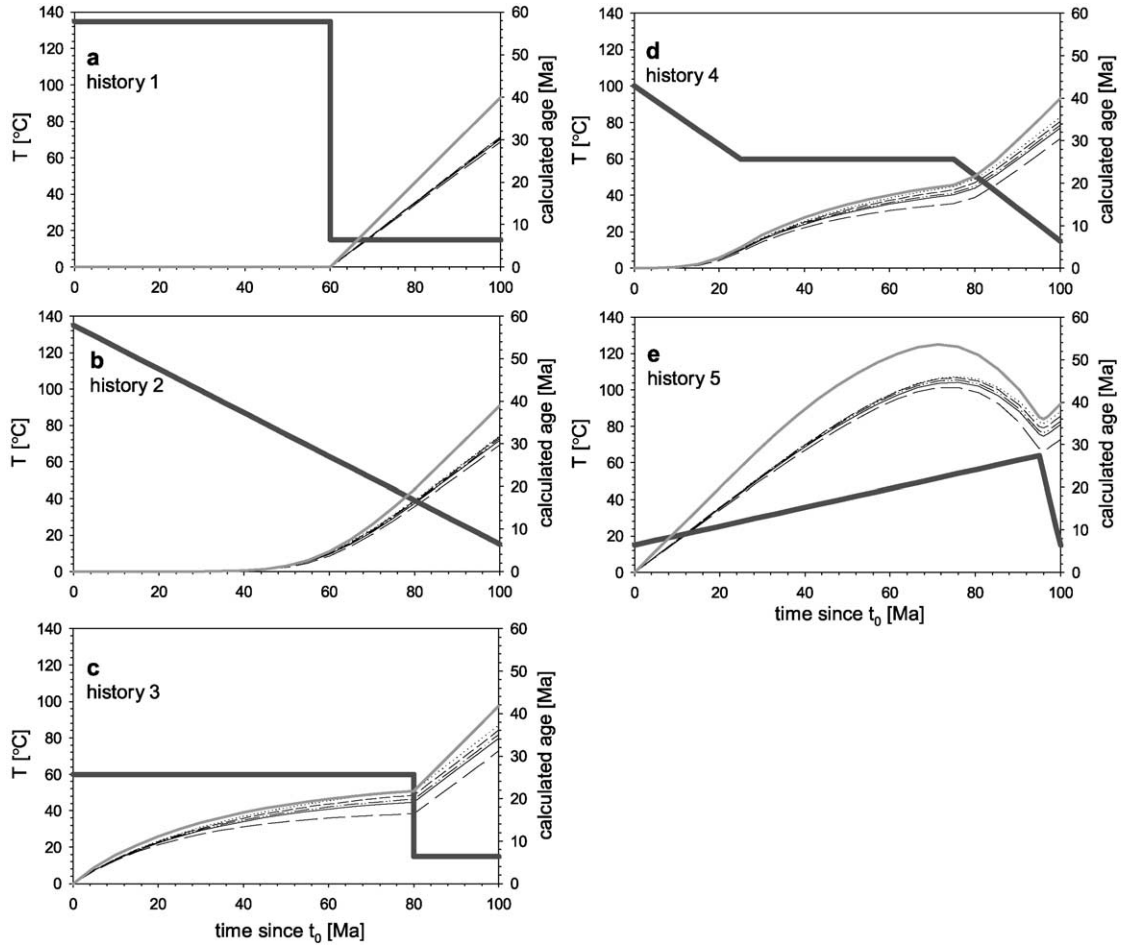

Fig. 3. Calculated ages, t_c, for various thermal histories. The thermal histories 1–5 (a–e) are depicted as thick dark grey lines and are the same as used by Wolf et al. (1998). The grey solid lines depict the evolution of a sphere without α-emission; all other evolution curves include α-emission. Solid line: sphere; dash–dotted line: finite cylinder; short dashed lines: rectangular block; long dashed lines: infinite cylinder; dotted line: cube. The sequence of calculated t_c's is always the same; in increasing order: infinite cylinder, sphere, finite cylinder, rectangular block, cube. The dimensions of the bodies are given in the text; all have identical surface to volume ratios.

case, diffusion essentially plays no role after the drop in temperature. The evolution is comparable to the one without α-ejection; however, the slope is reduced to 0.75 times its old value (=1), corresponding to the fraction F_T of α-particles retained in the crystal (see Eq. (5) with "=" sign). This value follows immediately from Eq. (26) for the case of the sphere. The fraction appears practically independent on the considered shape. These results are in agreement with the results of Farley et al. (1996), which were obtained along different lines (namely from retentivity calculations without considering diffusion and time series).

Fig. 3b shows the results for history 2, for which the temperature decreases fast, but not instantaneously through the zone of partial retention. Once the temperature decreased below 40 °C, t_cs are again 0.75 times the t_cs calculated without α-ejection. Also, for this history, diffusion has little effect on the results.

Fig. 3c shows the results for history 3, with the temperature staying in the partial retention zone for the first 80 Ma. Afterward, the temperature is low and the slope is again 0.75; however, the thermal history has its effect on the final t_c: this is not 0.75 times the value calculated without α-ejection, but considerably more than this (except for the infinite cylinder, which is an odd one out). This can be understood from the interplay of α-ejection and diffusion. In the new calculation, the He concentration in the outer parts of the crystal is depleted by α-ejection; however, in the old calculation, much more He was generated in the outer parts and, consequently, it was depleted by subsequent diffusion to a much greater extent than in the new calculation. As a consequence, the difference between the two resulting t_c is not a factor 0.75, but a factor much closer to one. This shows that a naive correction for α-ejection using a nondiffusive retentivity factor (as, e.g. in House et al., 1999; Stockli et al., 2000; Warnock et al., 1997) is incorrect once diffusion is important, i.e. if a sample remains for a significant period of time in the partial retention zone (PRZ, Wolf et al., 1998).

It is also seen in Fig. 3c that if the temperature is in the partial retention zone, results for different shapes (but same S/V ratio) become somewhat divergent, as was also seen when α-ejection was neglected (Part I). The results for the sphere, which are the easiest to obtain, are still a good approximation for the other finite shapes; however, they are systematically slightly too low. The infinite cylinder has a lower t_c than the finite shapes.

For histories 4 and 5 (Fig. 3d and e), about the same comments apply as for history 3. For the finite shapes, the retentivity is always considerably higher than 0.75 times the retentivity calculated without α-ejection. The mutual positions of the curves for various finite shapes are always the same, rising in the order sphere–cylinder–rectangular block cube. The curve for the infinite cylinder should be considered apart, and always lies below the curves for the finite shapes.

3.2. Results for zoned distribution of parent nuclides

It must be first explained how the zonal distributions are chosen. The crystal is divided into an inner and an outer zone, with the inner zone obtained by

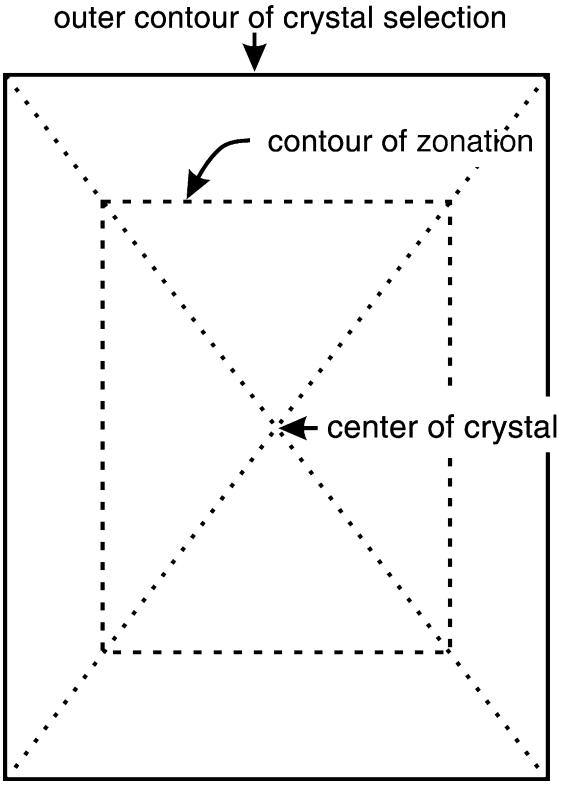

Fig. 4. Illustration of a zoning within a finite rectangular section of a crystal. The zone boundaries have the same center and shape as the crystal.

mathematically shrinking the crystal by some factor, keeping its center and shape unchanged (see Fig. 4). The distribution $U_{place}(x,y,z)$ for the source of α-particles is then chosen such that U_{place} is constant U_0 in either the inner or outer zone, whereas $U_{place}=0$ for the complementary zone. U_0 is determined by the requirement that the volume average of U_{place} is one (see Section 2.1). It is easily seen that U_0 is consequently a function of the shrinking factor, and independent on the shape, provided the shape is finite. The infinite cylinder obviously requires separate treatment, as it can shrink in only two instead of three directions. The considered shrinking factors are 2/3 and 5/6. With shrinking factor 2/3, one obtains for the inner and outer source $U_0=1/(2/3)^3$ and $U_0=1/(1-(2/3)^3)$, respectively, except for the infinite cylinder for which second powers instead of third powers should be used. Analogous expressions hold for factor 5/6.

We now compare the outcomes for the different zoning cases, for the five usual histories, but only for the spherical shape, for the moment. It will be shown below that the other shapes only yield small deviations, except for the infinite cylinder as usual. Re-

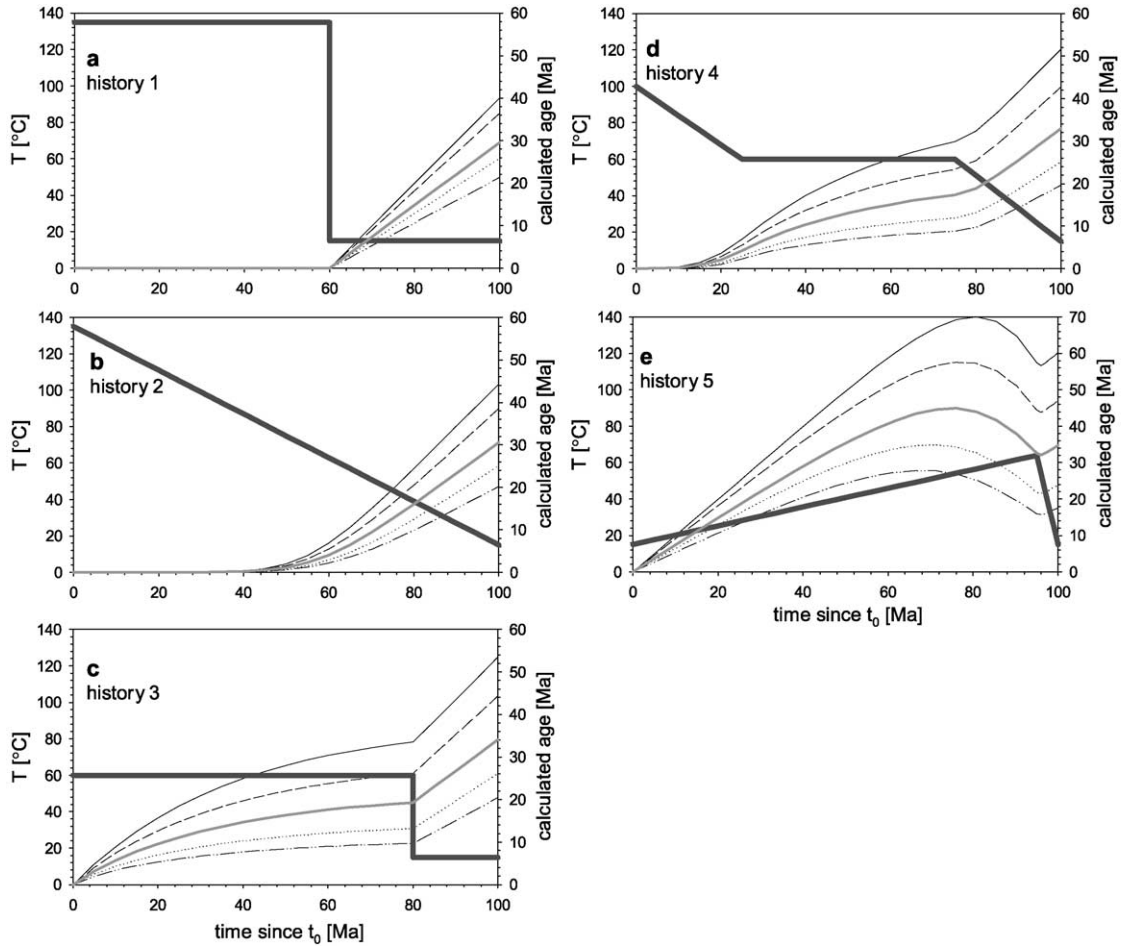

Fig. 5. Calculated ages, t_c, for various thermal histories including α-emission ($\sigma=20$ μm) for zoned and homogenous spheres ($a=60$ μm). The thermal histories 1–5 (a–e) are depicted as thick dark grey lines and are the same as used by Wolf et al. (1998). The grey solid lines depict the evolution of a sphere with homogenous distribution of the α-source. Solid line: source in inner 2/3; dashed line: source in inner 5/6; dotted line: source in outer 1/3; dash–dotted line: source in outer 1/6 of the crystal.

member that the radius of the sphere in these calculations is $a = 60$ μm and the stopping distance is $\sigma = 20$ μm.

Fig. 5a shows the results for history 1. Although the total α-production rate is the same for all cases, t_c is seen to depend strongly on the location of the source. The nearer the source is located to the outer world, the smaller t_c becomes. On the other hand, if the source is located entirely at a distance that is $\geq$ the stopping distance away from the outer world, as is the case with the source in the inner 2/3, there is full retentivity (so that the slope of t_c as a function of t is one).

Note that these results could again have been obtained directly from F_T, as diffusion is negligible. F_T can be calculated analytically, using the instructions of 2.6. Readers with interest in calculations may check that the results for the cases of innermost 2/3, 5/6, homogeneous distribution, and outermost 1/3, 1/6, are: $F_T = 1$, 0.91, 0.75, 0.65, 0.53. These are just the slopes of the corresponding curves in Fig. 5a.

The other four histories (Fig. 5b–e) show essentially similar results; however, the zoning dependence becomes even more spectacular as the effects of diffusion (corresponding to a slow passing of temperature through the PRZ) become more important. The reason is that diffusive loss is interwoven with α-emission. If the relative loss due to α-emission is larger, subsequent diffusive loss is relatively less efficient as both processes deplete the outer parts more that the inner parts. For history 5, the t_c for parent nuclides in the outer 1/6 is less than one third of the t_c for the same number of parent nuclei in the inner 2/3. These results show that the knowledge of spatial distribution of the He in a crystal is very important for interpreting values of t_c ("ages").

We now turn again to the important question whether a sphere can be used to approximate other crystal shapes. The specifications for the computations concerning the other shapes are as in Section 3.1. We must add for completeness that the calculations are somewhat less accurate than the previous ones since when the γ_n are determined numerically, the spatial features of the source distribution are somewhat more difficult to resolve than without zoning. An additional source of inaccuracy is the summation method: the growth of the partial sums Σ_M as a function of M (as defined in Part I) is less regular. This is illustrated in Fig. 6 ($\sum_M$ for finite cylinder, source in inner 2/3, first

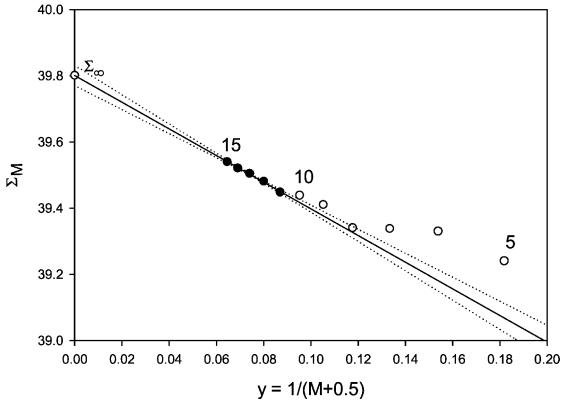

Fig. 6. Illustration of determining an infinite sum $\sum_\infty$ from partial sums $\sum_{11} \ldots \sum_{15}$. The dotted lines denote the 95% confidence envelope of the linear extrapolation. Discussion is given in the text.

history, time = 100 Ma). This irregularity is, in part, an immediate consequence of the zoning (inspection shows that it also occurred already to some extent for the sphere, for which exact values of γ_n were used). Fig. 6 shows that the error is small: for this special case since neither α-particles nor He atoms can leave the crystal, the exact outcome is known: $t_c = 40$ Ma. The calculated outcome is only 0.5% less than this. However, using lower order Σ_M would have resulted in a less accurate outcome.

Fig. 7 shows for history 1 how for each zone t_c depends on the shape. Apart from the infinite cylinder, the curves almost coincide. Results for history 2 (not shown) are similar. For history 3 (Fig. 8), there is a slight shape dependence for inner sources (Fig. 8a and c), comparable to the case with homogeneous distribution (see Section 3.1). On the other hand, for outer sources (Fig. 8b and d), the shape dependence is smaller. The same remarks hold for histories 4 (not shown) and 5 (Fig. 9). As for homogeneous distribution, for cases in which shape dependence occurs, the t_c for the sphere slightly underestimates the t_c for the other finite shapes, and overestimates the t_c for the infinite cylinder. The agreement between the finite cylinder and the sphere is very good, deviations are mostly $< 5\%$ (Figs. 7–9). This agreement is fortunate as the finite cylinder is currently the best approximation of the shape of a apatite crystal available.

In the examples depicted in Figs. 5–9, we have only considered parent nuclides distributions that can

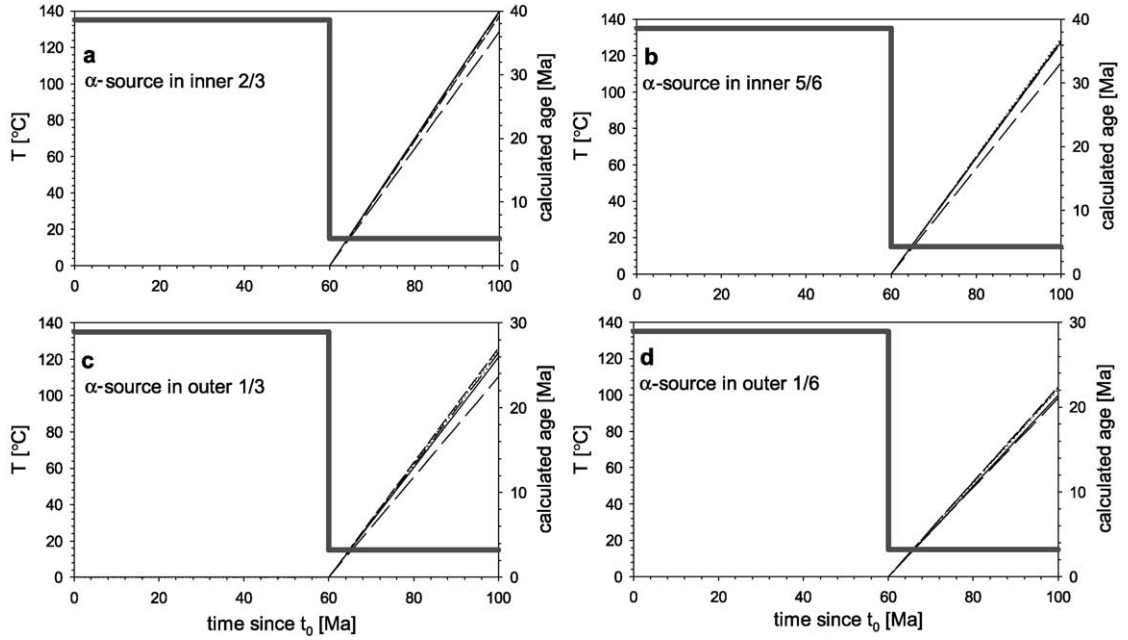

Fig. 7. Calculated ages, t_c, for thermal history 1 (Wolf et al., 1998) and various zoned crystal shapes. The results for the different zonations, α-sources in inner 2/3 and 5/6 and outer 1/3 and 1/6, are shown in (a)–(d). In these plots, solid lines denote sphere; dash–dotted lines: finite cylinder; short dashed lines: rectangular block; long dashed lines: infinite cylinder; dotted lines: cube. The dimensions of the bodies are the same as in Fig. 3; all have identical surface to volume ratios.

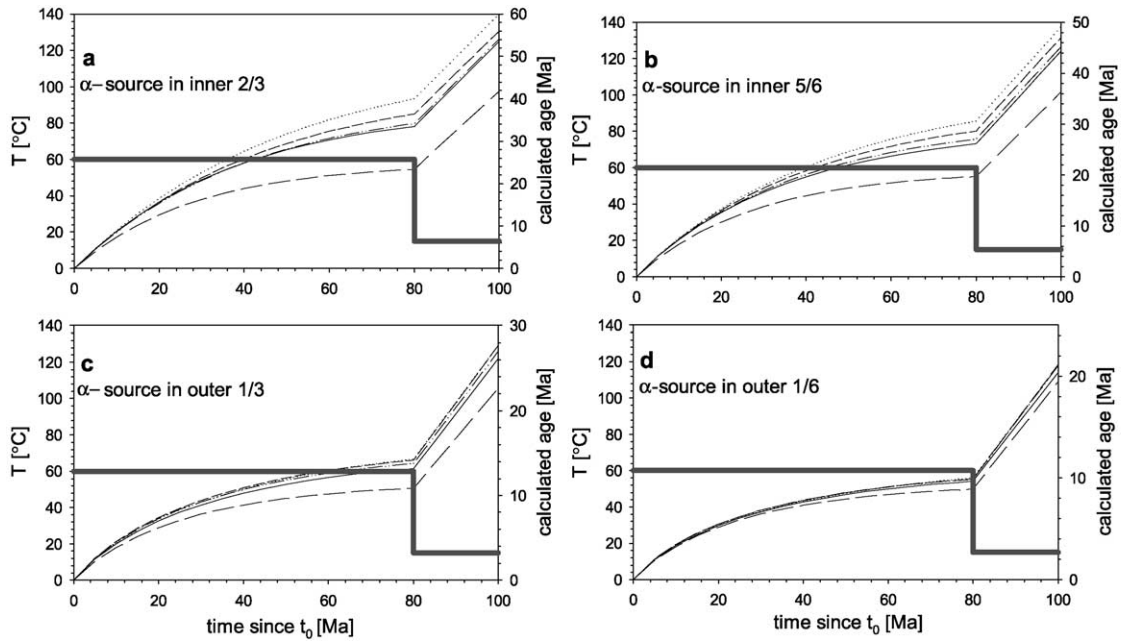

Fig. 8. Same as Fig. 7 but for history 3.

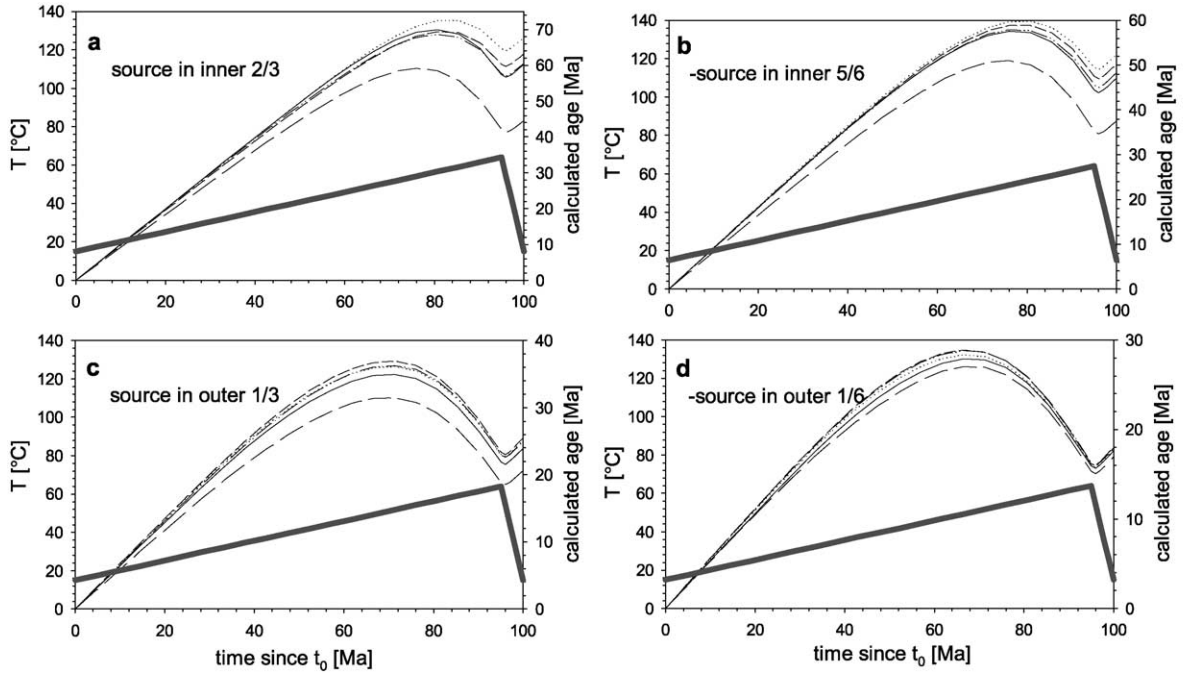

Fig. 9. Same as Fig. 7 but for history 5.

be described by a single step function. For cases with more complicated distributions that can be described as a combination of multiple step functions, results can be obtained by application of the superposition principle (Section 2.2). As follows from the superposition principle and the examples shown in Figs. 7–9, also the more complicated zonations can be ''translated'' into a spherical geometry for easy and fast calculation without significant sacrifice of computational accuracy.

4. Conclusions

In Part I (Meesters and Dunai, in press), a method has been developed to calculate predicted He contents in crystals, for application to (U–Th)/He thermochronometry. The method has been extended in the present paper to cases in which α-emission is important and in which the parent nuclides have eventually a zonal instead of homogeneous distribution.

The method is based on decomposition into eigenmodes. For each eigenmode, coefficients μ (eigenvalue) and γ have to be determined, the expressions depending on the crystal shape. For some shapes, determination of γ is difficult; however, for the special case of a spherical shape, analytical expressions are derived in this paper for both homogeneous and zonal distribution of the parent nuclides.

There is an important reason to pay special attention to spherical ''crystals''. The number of eigenmodes that have to be considered is typically 15 for spherical ''crystals'' (and for the infinite cylinder), 15^2 for the finite cylinder, and 15^3 for block-shaped crystals. Hence, spherical crystals are by far the most efficient from a computational point of view. This is important since in practice, e.g. for inversion of depth (altitude)–age profiles many runs with a model calculating He contents from thermal series have to be performed. For a successful inversion, many trial runs are needed to obtain a good fit. Fortunately, a comparison of calculated results shows that for crystals with modest aspect ration of varying shape, but with the same surface-to-volume (S/V) ratio, all yield very similar He age t_c (= He content divided by the rate of He production) in response to the same thermal

histories. This implies that it is possible to "translate" the problem for a crystal of a given shape, to a problem for a crystal with spherical shape. This remains so if zoning of the parent nuclides occurs, provided the corresponding zoning is imposed on the sphere.

In Section 3.1, results for homogeneous distribution of the parent nuclides are considered. For a thermal history in which the temperature drops suddenly from high to low (so that the diffusivity drops suddenly from effectively infinite to effectively zero), results are similar to those obtained earlier with a nondiffusive model by Farley et al. (1996). Once the diffusion has ceased, there is a retention factor (=retained fraction of α-particles) F_T that corresponds also to the He retention, and that can be calculated analytically for spheres.

However, very different results are obtained if the crystal stays during its cooling a long time in the PRZ. In this case, a model incorporating both diffusion and α-emission (like the present one) is required. Comparison reveals that, with α-emission, the retained fraction of He is not F_T times the retained fraction without α-emission, but considerably more than that. The reason is that it is not allowed to consider loss by α-emission and loss by He diffusion as independent processes: ejection of α-particles causes the outer parts more than the inner parts to be depleted in new He, and, hence, it diminishes in a sense the effect of diffusive loss since diffusive loss also pertains primarily to the He in the outer parts. In the literature, little attention has been paid hitherto to this problem of correcting for the combined effect of α-emission and diffusion. Model calculations are generally carried out by calculating diffusive loss without α-emission, and afterward multiplying the resulting He content with the nondiffusive F_T as calculated from Farley et al. (1996) (e.g. House et al., 1999; Stockli et al., 2000; Warnock et al., 1997). It follows from the foregoing that this can result in a substantial underestimation of the retentivity for samples that spent considerable time in the PRZ.

The results show that a sphere can be employed as an approximation of crystals with a different shape, but with the same S/V ratio. The retentivity of the sphere is only slightly smaller than the retentivity of the other shapes with modest aspect ratio. Calculations for infinite cylinders with the same S/V ratio yield somewhat more divergent results as compared to the sphere and other shapes and yields always lower values for t_c. This implies that one should be careful with approximations for very elongated shapes.

Calculations of situations where the parent nuclides are not homogeneously distributed in the crystal, but restricted to a zone (Section 3.2), show a strong dependence on the choice of the zoning. Retentivity is smaller as the parent nuclides are located closer to the outside. Moreover, if diffusion is significant, i.e. especially when protracted passage/storage in the partial retention zone does occur, the zoning dependence is even stronger. The t_c calculated for a given number of the parent nuclei contained in the outer part may be less than a third of the t_c calculated for the same number of parent nuclei in the inner part (same crystal size and shape, and same thermal history). The reason is that diffusion cooperates with α-emission in depleting the outer parts more than the inner parts. It follows from this that a thermo-chronological model should incorporate diffusion, α-emission, and zoning in a combined way.

In most cases, it is possible, in general, to "translate" the zoning in an arbitrary crystal to zoning in a spherical "crystal" with the same S/V ratio. As noted above, computations for spherical crystals are easier and faster than for other crystal shapes. A comparison has been made between results for spherical and other shapes and for crystals with modest aspect ratios a good agreement was found. From the principle of linear superposition, it follows that this agreement, found for simple single step zoning, is equally valid for cases with a more complicated zonal distribution of the parent nuclides. The agreement is best between spheres and finite cylinders (deviations mostly $<5\%$), which is fortunate as the shape of apatite is best approximated by a finite cylinder.

A user-friendly version of the program to perform calculations for spherical geometries as discussed in Part I and Part II is currently in preparation and can be obtained from the authors when it becomes available.

Acknowledgements

We are grateful for stimulating discussions with all the members of the fission track group at the Vrije Universiteit Amsterdam. Special thanks to Bart

Hendriks who directed our attention to zonation in apatites and provided the excellent photomicrographs and to Marlies ter Voorde for useful suggestions to make this paper more readable. The constructive reviews of Peter Zeitler and Ken Farley improved the manuscript considerably. This is NSG-publication # 20011004.

Appendix A. Calculations for cases with spherical symmetry

A.1. Determining S_{place} for the sphere

The quantities U_{place} and S_{place} have been defined in Section 2.1. In the following, it is assumed that U_{place} depends on the distance s to the crystal center alone.

Our first problem is to express S_{place}. The principle is as follows (Fig. 10): Let C be the center of the spherical crystal with radius a. Now S_{place} in a point P is the average of U_{place} over all points P' lying at a distance, σ, from P. It $P'$is outside the crystal, $U_{\text{place}}=0$ there. The function U_{place} depends by assumption only on the distance s of P' to the center C of the crystal. Thus:

$$S_{\text{place}}(x,y,z) = \frac{1}{4\pi}\int_0^{2\pi} d\varphi \int_0^{\pi} d\theta \sin\theta U_{\text{place}}(s). \tag{31}$$

It can be found that s depends on the angle θ (Fig. 10) as follows:

$$s = \sqrt{r^2 + 2\sigma r\cos\theta + \sigma^2}, \tag{32}$$

in which r is the distance of P to C.

The integral over φ yields a factor 2π (the integrated function does not depend on φ). The integration over θ can be replaced with integration over s as a new variable (with r kept constant). Since:

$$\mathrm{d}s = -\frac{\sigma r}{s}\sin\theta \mathrm{d}\theta, \tag{33}$$

and $s(\theta=0)=r+\sigma$ and $s(\theta=\pi)=|r-\sigma|$, this yields the simple expression:

$$S_{\text{place}}(x,y,z) = \frac{1}{2\sigma r}\int_{|r-\sigma|}^{r+\sigma} \mathrm{d}s\ sU_{\text{place}}(s). \tag{34}$$

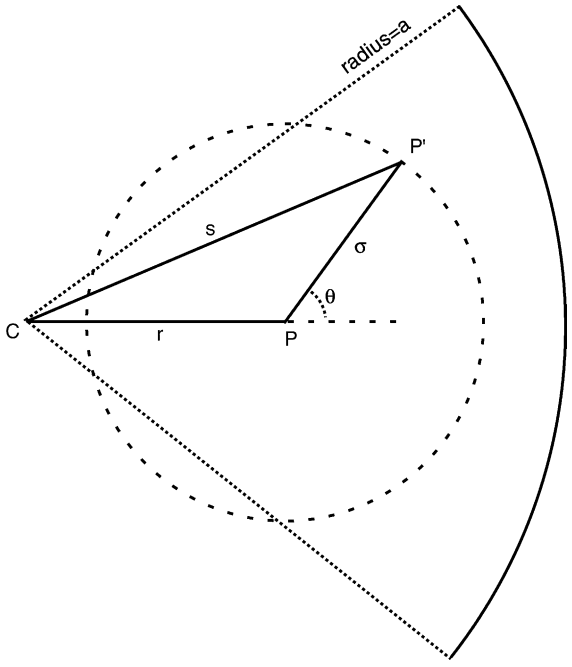

Fig. 10. Explanation of the symbols used for the calculation of S_{place} for the sphere.

A.2. Determining γ_n and F_T for the sphere

The next problem is to determine from this (see Section 2.4):

$$\gamma_n = (-1)^{n+1}\frac{6}{(n\pi)}\frac{1}{a^2}\int_0^a \mathrm{d}r\ r^2 S_{\text{place}}(r)\mu_n(r), \tag{35}$$

in which:

$$\mu_n(r) = \frac{1}{r}\sin\left(\frac{n\pi}{a}r\right), \tag{36}$$

and:

$$F_{\mathrm{T}} = \frac{3}{a^3}\int_0^a \mathrm{d}r\ r^2 S_{\text{place}}(r). \tag{37}$$

After substituting the expression (34) for S_{place}, the expressions for F_{T} and γ_n are double integrals. It is

easier to reverse the order of integration, so that the inner integral can be carried out already without knowledge of the arbitrary function $U_{\text{place}}(s)$. This yields the still complicated forms:

$$\gamma_n = (-1)^{n+1}\frac{3}{n\pi} \times \frac{1}{\sigma a^2}\int_0^a \mathrm{d}s\ sU_{\text{place}}(s) \times \int_{|s-\sigma|}^{\min(s+\sigma,a)} \mathrm{d}r \sin\left(\frac{n\pi}{a}r\right), \tag{38}$$

and:

$$F_{\text{T}} = \frac{3}{2\sigma a^3}\int_0^a \mathrm{d}s\ sU(s)\int_{|s-\sigma|}^{\min(s-\sigma,a)} \mathrm{d}r\ r, \tag{39}$$

it being understood that the integral over r is replaced with zero in case the "lower" bound $|s-\sigma|$ is larger than the "upper" bound $\min(s+\sigma,a)$. On working out all possible cases, it is found that the prescript for the double integration depends as follows on the ratio of σ to a: for $\sigma < a$, there are two terms:

$$\int_0^{a-\sigma} \mathrm{d}s \int_{|s-\sigma|}^{s+\sigma} \mathrm{d}r \ldots + \int_{a-\sigma}^{a} \mathrm{d}s \int_{|s-\sigma|}^{a} \mathrm{d}r \ldots, \tag{40}$$

for $a \le \sigma < 2a$, there is only one term:

$$\int_a^{\sigma-a} \mathrm{d}s \int_{\sigma-s}^{a} \mathrm{d}r \ldots, \tag{41}$$

and for $\sigma \ge 2a$, the expression becomes zero.

References

Carslaw, H.S., Jaeger, J.C., 1959. Conduction of Heat in Solids. Clarendon Press, Oxford, 510 pp.

Collins, R.E., 1968. Mathematical Methods for Physicists and Engineers. Reinhold, New York.

Farley, K.A., 2000. Helium diffusion from apatite: general behaviour as illustrated by Durango fluorapatite. J. Geophys. Res. 105 (B2), 2903–2914.

Farley, K.A., Wolf, R.A., Silver, L.T., 1996. The effects of long alpha-stopping distances on (U–Th)/He ages. Geochim. Cosmochim. Acta 60, 4223–4229.

House, M.A., Farley, K.A., Kohn, B.P., 1999. An empirical test of helium diffusion in apatite: borehole data from the Otway basin, Australia. Earth Planet. Sci. Lett. 170, 463–474.

Meesters, A.G.C.A., Dunai, T.J., 2002. Solving the production–diffusion equation for finite diffusion domains of various shapes: Part I. Implications for low-temperature (U–Th)/He-thermochronology. Chem. Geol., in press.

Stockli, D.F., Farley, K.A., Dumitru, T.A., 2000. Calibration of the apatite (U–Th)/He thermochronometer on an exhumed fault block, White Mountains, California. Geology 28, 983–986.

Warnock, A.C., Zeitler, P.K., Wolf, R.A., Bergman, S.C., 1997. An evaluation of low-temperature apatite U–Th/He thermochronology. Geochim. Cosmochim. Acta 61, 5371–5377.

Wolf, R.A., Farley, K.A., Kass, D.M., 1998. Modeling of the temperature sensitivity of the apatite (U–Th)/He thermochronometer. Chem. Geol. 148, 105–114.

Ziegler, J.F., 1977. Helium stopping powers and ranges in all elemental matter. The Stopping and Ranges of Ions in Matter. Pergamon, New York, p. 4, 367 pp.